# Scientific Highlights

## Index

# Molecules behaving like atoms

M. Feng, J. Zhao, and H. Petek
Science 320, 359 (2008)

A team from the University of Pittsburgh and Donostia International Physics Center discovered atom like molecular orbitals of hollow molecules. In a scanning tunneling microscopy (STM) study of $C_{60}$ molecule, a hollow cage of sixty carbon atoms in the shape of a soccer ball, they found images suggesting that under some circumstances hollow molecules can exhibit electronic properties that mimic atoms. When several such molecules are combined into linear chains or close-packed islands, electrons injected into atom-like molecular orbitals delocalize as they would in a metal.

**The characteristic properties** of conductivity and reflectivity arise from the propensity of metal atoms to give up their electrons. If organic molecules could learn the same trick, they could become versatile components of molecule-based electronics. The team found that hollow molecules, such as $C_{60}$, behave as superatoms: at certain bias voltages they bind added electrons not to individual atoms, like other molecules, but to their empty core, giving them appearance of large atoms in STM images. When two hollow molecules come together, their images resemble those of diatomic molecules. For larger one- or two-dimensional aggregates the images resemble free-electron alkali metals. The atom-like properties of $C_{60}$ molecules are reproduced by density functional theory calculations.

The theoretical modeling suggests that the origin of superatom states are the image potential states of a two-dimensional carbon sheet, graphene. Such image potential states were discovered and have been studied for metals and liquid He in the pioneering theoretical work of Pendry and Echenique. The superatom states are derived form the image potential states of graphene through a topological distortion into a sphere. The discovery of superatom states in $C_{60}$ molecules provides the first experimental and theoretical verification of image potential states of molecular sheets. The attribution of superatom states to the universal origin in the image potential states of a molecular sheet suggests that hollow molecules of other materials should exhibit similar properties, and it suggests new strategies for design of novel molecular electronic materials.


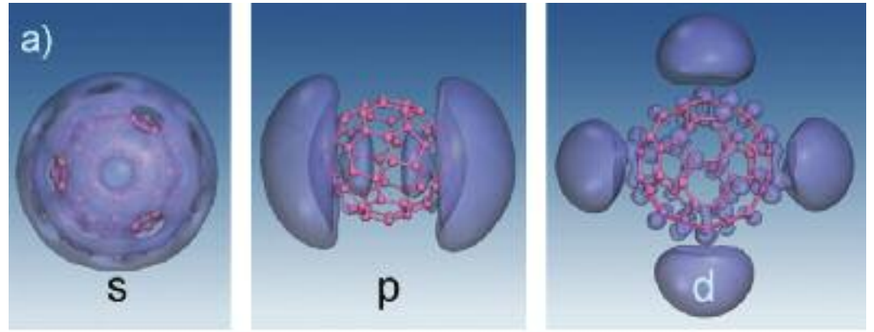


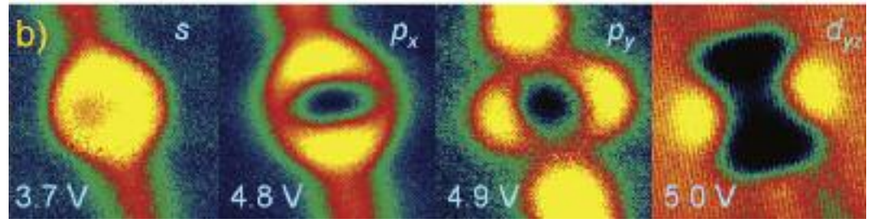


a) The theoretical and b) experimental images of the superatom orbitals of $C_{60}$ molecule. The theoretical images indicate the existence of unoccupied orbitals of $C_{60}$ and other hollow molecules with spatial distributions of *s*, *p*, *d*, ... symmetry spherical harmonic orbitals of atoms, corresponding to orbital angular momentum $l$=0, 1, 2.... Molecular orbitals with distinctly atom-like s, p, and d character have been discovered through spectroscopic imaging in a low temperature STM.

The discovery of superatom states in $C_{60}$ molecules provides the first experimental and theoretical verification of image potential states of molecular sheets.

# High-level correlated approach to the jellium surface energy, without uniform-electron-gas input

L.A. Constantin, J.M. Pitarke, J.F. Dobson, A. Garcia-Lekue, and J.P. Perdew
Physical Review Letters 100, 116102 (2008)

We resolve the long-standing controversy over the metal surface energy: Density-functional methods that require uniform-electron-gas input agree with each other, but not with high-level correlated calculations such as Fermi-hypernetted-chain and diffusion-Monte-Carlo calculations that predict the uniform-gas correlation energy accurately. Here we apply the inhomogeneous Singwi-Tosi-Land-Sjölander method, and find that the density functionals are indeed reliable. Our work also vindicates the use of uniform-gas-based nonlocal kernels in time-dependent density-functional theory.

**Density-functional theory** (DFT) provides ground-state electron densities and energies [and, in its time-dependent version (TDDFT), excitation energies] for atoms, molecules, and solids. Because of its simple self-consistent-field structure, DFT is used for electronic-structure calculations almost exclusively in condensed matter physics, and heavily in quantum chemistry. Exact in principle, the theory requires in practice approximations for the exchange-correlation (xc) energy (and the socalled xc kernel of TDDFT) as a functional of the density. All commonly used nonempirical approximations require input from the uniform electron gas, which is transferred to inhomogeneous densities. The reliability of these approximations must be judged a posteriori, and there had been for many years a long-standing puzzle related to their reliability for solid surface energies, with implications for vacancies and clusters. The surface energy is not only of technological importance, but also a classic and highly sensitive test case for theories of exchange and correlation in manyelectron systems.

Here we develop a very high-level correlated many-body approach that generalizes the well-known orbital-based Singwi-Tosi-Land-Sjölander (STLS) formalism to the case of inhomogeneous systems, and we resolve the long-standing controversy over the reliability of existing densityfunctional calculations of metal surfaces energies. Our calculations lead us to the conclusion that the existing DFT calculations are reliable (in contrast with the then available high-level correlated Fermi-hypernetted-chain and diffusion-Monte-Carlo calculations). An analysis of the surface energy into contributions from dynamical density fluctuations of various two-dimensional (2D) wave vectors is also reported, which rules out the belief that the local-density approximation for the particle-hole interaction (in the context of TDDFT) might be inadequate for the description of the surface energy of simple metals.

We resolve the long-standing surface-energy controversy.

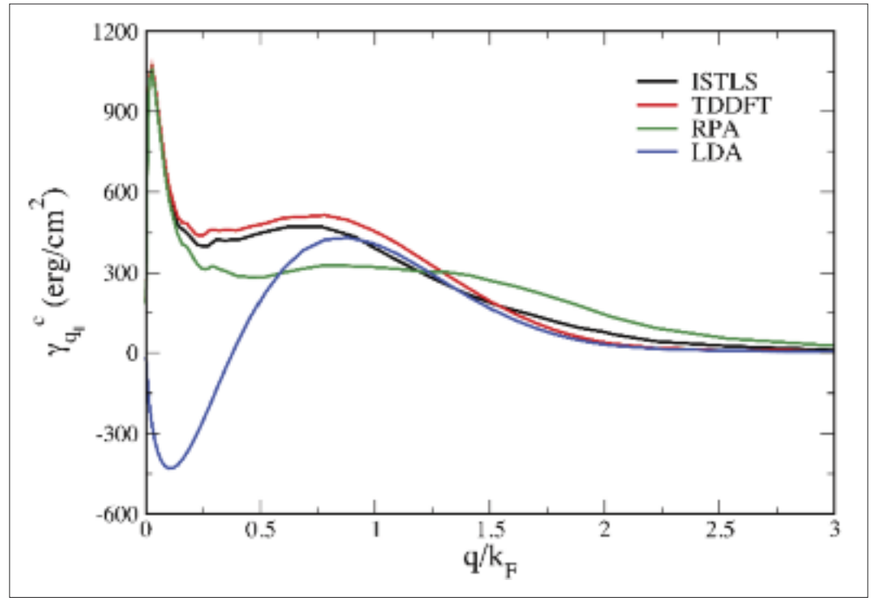


2D wave-vector analysis of the correlation surface energy of a jellium slab of thickness 7.21 $r_s$ ($r_s$ = 2.07). Black, red, green, and blue lines represent inhomogeneous-STLS (ISTLS), uniform-gasbased TDDFT, random-phase-approximation (RPA), and local-density-approximation (LDA) calculations, respectively. $q$ is the magnitude of the 2D wave vector (in the surface plane) of the density fluctuations. The area under each curve amounts to the correlation surface energy in units of erg/cm$^2$. $k_F$ represents the magnitude of the Fermi wave vector. $r_S$ represents (in units of the Bohr radius) the radius of a sphere that encloses one electron on average. We observe that in the longwavelenght limit (small $q$) both ISTLS and TDDFT calculations coincide with the RPA, which is exact in this limit, while the LDA fails badly. In the large-$q$ limit, both ISTLS and TDDFT calculations approach the LDA, as expected, while the RPA is wrong. Two independent schemes (the ISTLS approach, which does not use and isotropic xc kernel derived from the uniform gas, and the TDDFT approach, which uses a uniform-gas-based isotropic xc kernel) yield essentially the same wave-vector analysis of the correlation surface energy. This supports the conclusion that the local-density approximation for the particle-hole interaction is indeed adequate to describe simple metal surfaces.

Our work vindicates the use of uniform-gas-based nonlocal kernels in time-dependent density-functional theory.

# Role of electron-hole pair excitations in the dissociative adsorption of diatomic molecules on metal surfaces

J.I. Juaristi, M. Alducin, R. Díez Muiño, H.F. Busnengo, and A. Salin
Physical Review Letters 100, 116102 (2008)

**The role of electronic excitations in the dissociation of molecules at metal surfaces has been studied. The validity of the Born Oppenheimer approximation to describe this kind of processes has been proven.**

**The Born-Oppenheimer approximation** is the usual starting point in the theoretical study of the interaction of thermal molecules with surfaces. Among other things, this approximation involves to neglect the energy loss suffered by the molecule along its trajectory as a consequence of the electronic excitations that it induces in the metal. Paradoxically, the experimental evidence of these excitations is such that their existence is out of question. The great controversy in this field is related to the question of which is the real importance of electronic excitations to determine the dissociation of the molecules or, more generally, the reactivity of the molecules at surfaces. With the aim of gaining knowledge on this question, a theoretical model has been developed, totally based on *ab initio* calculations, which also incorporates the electronic excitations into the dynamic equations. The contribution of electron-hole pair excitations to the reactive dynamics of $H_2$ on Cu(110) and $N_2$ on W(110) has been evaluated, including the six dimensionality of the process in the entire calculation. The interaction energy between molecule and surface is represented by an *ab initio* six-dimensional potential energy surface. Electron friction coefficients are calculated with density functional theory in a local density approximation. The two systems that have been considered represent two cases in which the dissociation dynamics is completely different. In $H_2$/Cu(110), the dissociation is ruled by a late activation barrier, at short distances from the surface. It is at these distances where the molecule finds high electron densities and where larger energy losses are more likely to occur. On the other hand, in $N_2$/W(110), the dynamics is more involved and combines direct and trapping mediated dissociation mechanisms. The dissociation of $N_2$ on metal surfaces has been considered as an emblematic example of a system where electronic friction can be relevant. The reasoning behind that assumption was the high value of the friction coefficient for N atoms moving in electronic media.

The results of our calculations showed that the contribution of electron excitations is a marginal correction to the dissociation dynamics and, therefore, that an adiabatic calculation is still meaningful for a wide range of situations. It was also shown that the low velocity of the reacting molecules in the surface regions of high electronic density is the main reason to explain this fact. This leads us to conclude that the theoretical models based on the Born-Oppenheimer approximation capture the main physics of the adsorption dynamics for these systems.

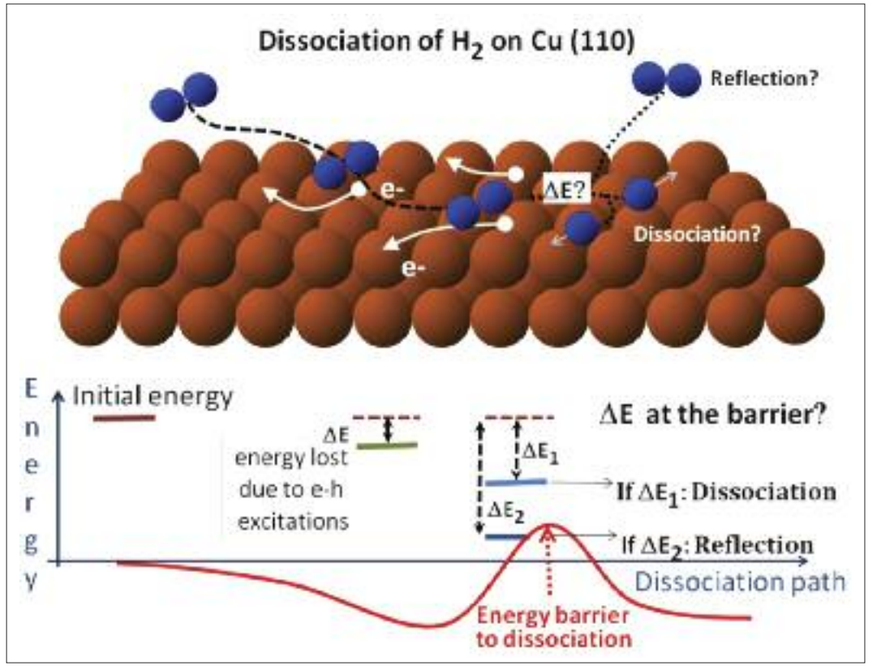


Figure 1. Schematic representation of the energetics of the interaction and the dynamics of $H_2$ at Cu(110).

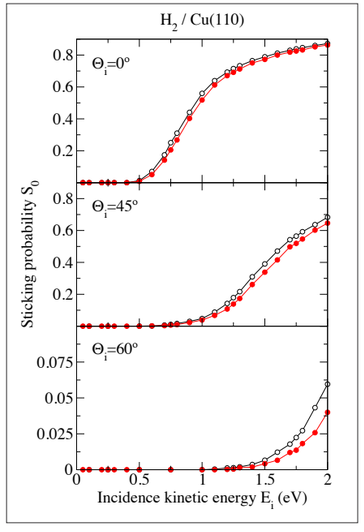


Figure 2. Dissociative sticking probability for $H_2$/Cu(110) at different incident angles. Full red (open black) circles are the results with (without) electronic friction.

We calculate for the first time the contribution of the electronic excitations to the dissociation of diatomic molecules at metal surfaces keeping the six dimensionality of the problem in the whole calculation.

# Formation of dispersive hybrid bands at an organic-metal interface

N. Gonzalez-Lakunza, I. Fernández-Torrente, K.J. Franke, N. Lorente, A. Arnau, J.I. Pascual
Physical Review Letters 100, 156805 (2008)

**A combined STS and DFT study of the interface between the monolayer of donor-acceptor TTF-TCNQ complex and a Au(111) substrate reveal that organic-metal dispersing hybrid bands, that have both metal and molecular character, are formed at the interface as a result of a complex mixing between molecular orbitals, mainly through TTF, and metal states. These results suggest that, by tuning the components of such molecular layers, the dimensionality and dispersion of organic-metal interface states can be engineered.**

**The use of organic thin films** in electronic devices requires the existence of electronic bands with high conduction properties, but, organic materials inherently have narrow bands and low electron mobility due to their weak intermolecular interactions. Organic-inorganic hybrid materials have been proposed as the ideal framework to merge the high carrier mobility of metals with the advantageous properties of organic materials. However, this approach remains sustained in empirical bases. A molecular scale conceptual picture of the cross talk between organic and metallic states in the formation of organic-metal (OM) hybrid bands is still missing.

Scanning tunneling microscope (STM) experiments, carried in ultrahigh vacuum and low temperature, show that TTF and TCNQ deposited on Au(111) self-assemble into mixed domains of alternating rows of donor and acceptor species with a 1:1 stoichiometry. In contrast to the TTF-TCNQ molecular solid bulk phase where molecules are $\pi$-stacked, here they lie parallel to the surface, as we can determine from their intramolecular structure [Fig. 1a)]. Such adsorption structure is confirmed by first principles calculations. The relaxed geometry of the TTF-TCNQ layer on Au(111) [Fig. 1b)-c)] shows that the molecular layer is bonded to the gold substrate trough the TTF. However, the most interesting properties of this OM system are revealed by scanning tunneling spectroscopy (STS) measurements.

In this work [1], we show that OM hybrid bands are formed at the interface between the donor-acceptor TTF-TCNQ complex and the Au(111) substrate. The bands combine a reduced dimensionality imprinted by the overlayer structure with a large dispersion reminiscent of its metallic character. By means of a combined STS and density functional theory (DFT) study [Fig. 2], we find that the bands originate from a complex mixing of metal and molecular states. While the TCNQ is essentially unperturbed by the underlaying surface, the TTF is hybridized with the Au(111) surface. The result is the formation of two interface bands with both molecular and metal character. They exhibit a free-electron metal-like dispersion and the anisotropic structure of the molecular layer.

This study allows us to obtain a conceptual understanding about the formation of OM hybrid bands. Our results suggest that tuning the strength of donor-metal interaction or spacing between the TTF rows may allow one to engineer the organic-inorganic interface band structure and, hence, the functionality of the molecular thin film.

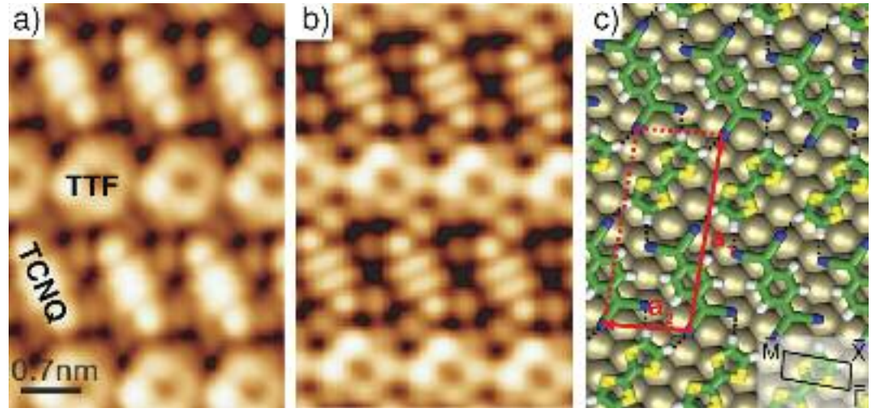


Figure 1. a) STM image with intramolecular resolution of the TTF-TCNQ mixed domain (V = 0.3 V; I = 0.4 nA). The molecular structure of TTF and TCNQ resembles the shape of the respective HOMO and LUMO. b) Simulated constant current STM image (V = 1.0 V) using the Tersoff-Hamman approach on the DFT optimzed geometry shown in c). c) The vectors a1 and a2 define the commensurate surface unit cell and the inset correspond to the SBZ.

An electronic band with quasi 1D dispersion is found at the metal-organic interface.

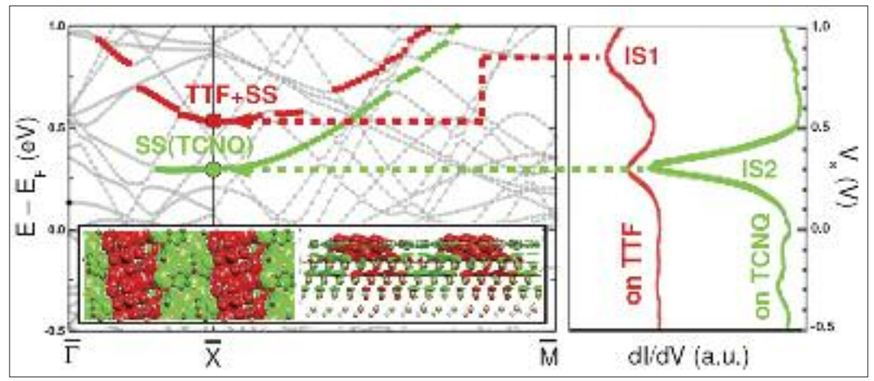


Figure 2. At the left part, the calculated band structure of TTF-TCNQ on Au(111) is shown, where the states that have some interface character has been coloured. Two bands can be distinguished: in green, a band that disperses along the molecular rows, and that has mainly metal character as it can be seen in the spatial charge distribution at Γ shown in the inset; and in red, a band with a bi-dimensional dispersion, mix of TTF and Au. At the right part, the experimental STS spectra taken onto TTF, in red, and onto TCNQ, in green, show two distinct features, IS1 and IS2, that are associated to the two calculated interface bands.

# Resonant plasmonic and vibrational coupling in a tailored nanoantenna for infrared detection

F. Neubrech, A. Pucci, T. W. Cornelius, S. Karim, A. Garcia-Etxarri, and J. Aizpurua
Physical Review Letters 101, 157403 (2008)

**A novel resonant mechanism involving the interference of a broadband plasmon with the narrow-band vibration from molecules is presented. With the use of this concept, the authors demonstrate experimentally the enormous enhancement of the vibrational signals from less than one attomol of molecules on individual gold nanowires, tailored to act as plasmonic nanoantennas in the infrared.**

**Vibrational spectroscopy of molecules** is of general importance in natural sciences, medicine, and technology. Direct infrared (IR) observation of molecular vibrations from a reduced number of molecules is a current challenge in all these fields. The respective sensitivity can be increased by several orders of magnitude with the use of surface-enhanced scattering techniques such as surface-enhanced Raman scattering (SERS) and surface-enhanced IR absorption (SEIRA).

In this study, the authors make use of IR antennas to boost the sensitivity of a SEIRA experiment. An IR antenna is a metallic nanostructure that acts as an effective receiver and transmitter of infrared light. It has the ability to confine the incident electromagnetic radiation to tiny spots of nanometer-scale dimensions (hot spots). This nanoscale concentration of the light permits to sense a much smaller amount of molecules than a regular SEIRA experiment.

This work shows both theoretical and experimentally that the effect of the resonant coupling of an individual plasmonic IR nanoantenna with the vibrational excitation of small number of molecules produces a different type of resonant SEIRA with unprecedented signal enhancement of 5 orders of magnitude, which means attomol sensitivity. The enhancing effect occurs only when the resonant interaction between both excitations (antenna and molecular vibration) is achieved, as proven by calculations.

To achieve a completely resonant situation, the length L of the nanoantenna is designed to hold a plasmonic resonance exactly matching the spectral position of the vibrational fingerprints of the molecules. Because of the finite negative value of the dielectric response of gold in the IR, antenna resonances in the μm range of the spectrum appear for slightly shorter L than the ideal half-wave dipole antenna length. With help of exact EM calculations, carried out by the nanophotonics group of the DIPC, that correctly predict the spectral resonance position of such a system, the authors are able to engineer the geometrical characteristics of the nano-antenna to obtain the resonance at the required IR wave- length and measure the vibrational signal of the molecules with unprecedent sensitivity.

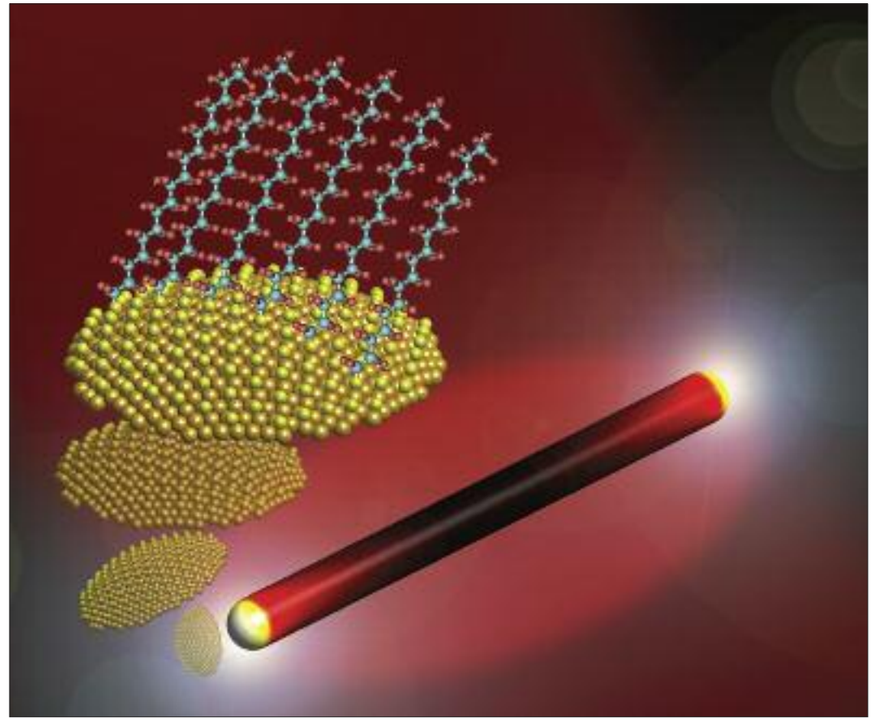

Figure 1. Sketch showing the experimental setup. A monolayer of octadecanthiol (ODT) molecules is deposited on a single IR resonant antenna. The system is illuminated with light polarized parallel to the antenna axis, and the transmittance of the system is measured.

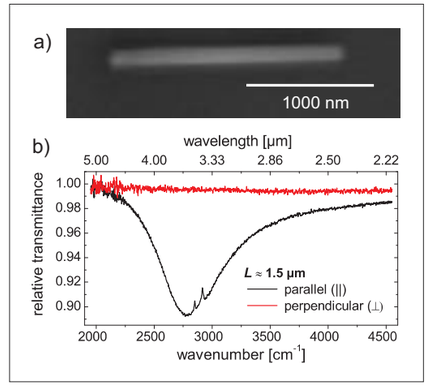


Few thousand molecules detected employing an IR nanoantenna as a near-field enhancing mechanism.

Figure 2. a) Scanning electron micrograph of a gold NW with similar dimensions as used in this study.
b) Relative IR transmittance in the spectral region of the fundamental resonance of a gold NW with one ODT monolayer for parallel ( || ) and perpendicular polarization ( ⊥ ). A CaF2 substrate is used. The broadband plasmonic resonance is observed around λ≈3.6μm.

# Complex quasiparticle structure induced by electron-phonon interaction: band splitting in the 1x1H/W(110) surface

Asier Eiguren and Claudia Ambrosch Draxl
Physical Review Letters 101, 036402 (2008)

We show that the self-consistent solution of the complex Dyson equation for the electron-phonon (EP) problem introduces many body effects which are often observed in photoemission experiments. The formalism is applied to the H covered W(110) surface, using first-principles results for the electronic and vibrational structure. We demonstrate that the measured spin-polarized surface band splitting [Phys. Rev. Lett. 84, 2925 (2000); 89, 216802 (2002)] can be traced back to different quasiparticle (QP) states induced by EP coupling. Despite the breakdown of the single QP picture, the spectral functions are very well represented by the predicted multiple QP structure.

**Recent developments in** angle-resolved photoemission spectroscopy (ARPES), revealing subtle details of the electronic structure, pose a challenge for a proper theoretical interpretation. Many 2D systems exhibit peculiarities in the measured spectral functions which are far from the ideal Lorentzian shape. Such observations include materials as different as bulk graphite and high-Tc cuprates and one clear possible origin can be found in electron-phonon (EP) coupling. This interaction is usually more pronounced in low dimensions, one prominent example being the hydrogen covered W(110) surface. In this system, for one of the surface states, experiment indicates the occurrence of two clear structures in the ARPES spectra, both with well defined energy dispersion [1]. Thereby, isotope substitution provided striking evidence for EP interaction being the source for the band splitting. The fact that the surface states are spin polarized as well as spin-orbit (SO) split, adds more interesting features to this already puzzling situation. We have included the spin-orbit interaction in the unperturbed electron structure calculation.

In this work we show that electron-phonon interaction indeed leads to multiple quasiparticle (QP) states. The key point is that the electron self-energy is not only a complex function, but also a complex function of complex (energy) argument. Indeed, we show that the analytic continuation to complex energies is not trivial. In this way, a complex Dyson equation can be defined for complex quasiparticle poles, which can be considered as self-consistently renormalized. Technically, our method is an important extension of Engelsberg and Schrieffer work [Phys. Rev. 131, 993], to finite temperatures and for generic Eliashberg functions.

An application to the 1x1H/W(110) surface demonstrates that several experimentally observed quasiparticle states are present in the calculation, offering an explanation detected many-body band splitting in photoemission measurements.

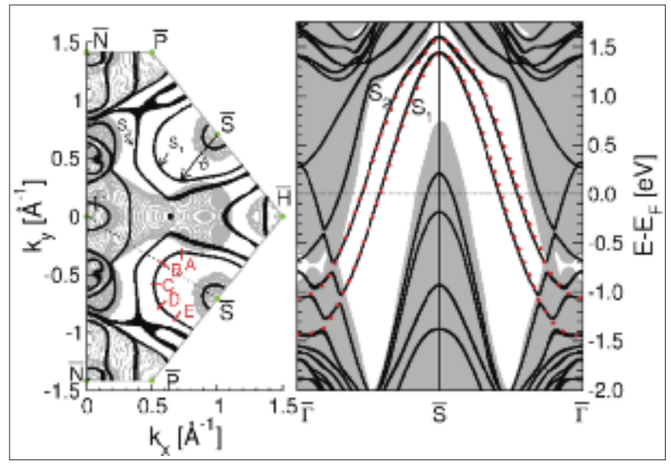


Left: Fermi surface of the slab system. Right: electron bands along $\bar{\Gamma}\,\bar{S}$, the grey area indicating the projected bulk bands. Red dots highlight the $S_1$ and $S_2$ bands.

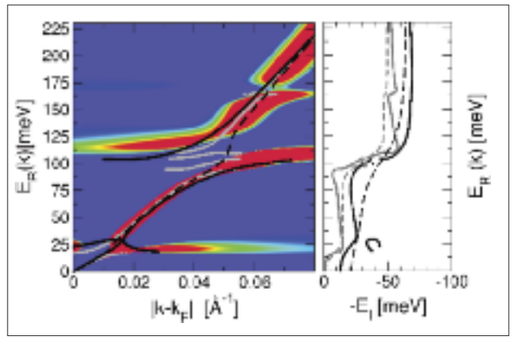


Self-consistent solution of the complex Dyson equation for H/W(110). Left: QP bands (solid lines) at $T$=150K (black) and 40K (grey). The background color presents the second derivative of the spectral function at $T$=40K. Right: inverse lifetimes $1/\tau = |\,E_I\,|$ (solid) and bare self-energies $1/\tau^0 = |\,\Sigma_I\,|$ (dashed) at T= 40K (grey) and T=150K (black).

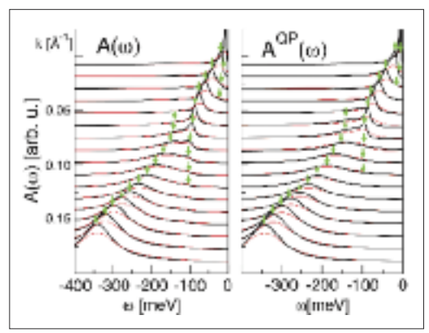


Spectral functions, $A_k$ (ω), at $T$=40K (thick black) and $T$=150K (thin red) of H/W(110) for different momenta compared to their counterparts in the multiple quasiparticle approximation, $A_k^{QP}(E) \equiv \sum_n \mathrm{Im}\left[\frac{-Z^{qp}(k,n)/\pi}{E - E^{qp}(k,n)}\right]$.

# Entangledlike chain dynamics in nonentangled polymer blends with large dynamic asymmetry

A. J. Moreno and J. Colmenero
Physical Review Letters 100, 126001 (2008)

**Simulations of a nonentangled polymer blend with large dynamic asymmetry reveal novel features for chain relaxation of the confined fast component. The latter strongly resemble usual observations for entangled homopolymers. We suggest a more general frame, beyond reptation models, for dynamic features usually associated to entanglement effects.**

**We have performed molecular dynamics** simulations on a simple model for polymer blends (Figure 1). The selected values for the chain length N are in all cases much smaller than the entanglement length of the corresponding homopolymer. A large dynamic asymmetry between the two components in the blend induces strong confinement effects for the fast component. At odds with standard predictions of the Rouse model, strong nonexponential behaviour for the Rouse normal modes is observed for the confined fast component. From simple scaling arguments we infer that strong nonexponentiality is an intrinsic feature which does not arise from a simple distribution of elementary exponential processes. Despite simulated chains being much shorter than the entanglement length, strong dynamic asymmetry induces dynamic features, as anomalous scaling properties for the Rouse modes (see Figure 2), resembling observations in strongly entangled homopolymers. Very recent simulations of chemically realistic blends [Brodeck et al., Macromolecules, to be published] confirm this observation, suggesting that this is a general feature of polymer blends with large dynamic asymmetry.

This unusual behaviour is associated to strong memory effects which break the Rouse-like assumption of time uncorrelation of the external forces acting on the tagged chain. The observed anomalous scaling laws for the Rouse modes strongly resemble predictions from recent theoretical approaches based on generalized Langevin equations (GLE). Within the approach of renormalized Rouse models for the memory kernel, nonexponentiality and anomalous scaling are directly connected to slow relaxation of density fluctuations around the tagged chain. The latter may be induced by entanglement, but data reported here for the fast component suggest that this is not a necessary ingredient. Analogies with entangledlike dynamics are indeed observed even for N = 4 monomers, provided that dynamic asymmetry in the blend is sufficiently strong.

The results of this work suggest a more general frame, beyond usual reptation-based models, for chain relaxation features usually associated to entanglement effects. They also open new possibilities for the application of GLE methods in complex polymer mixtures.

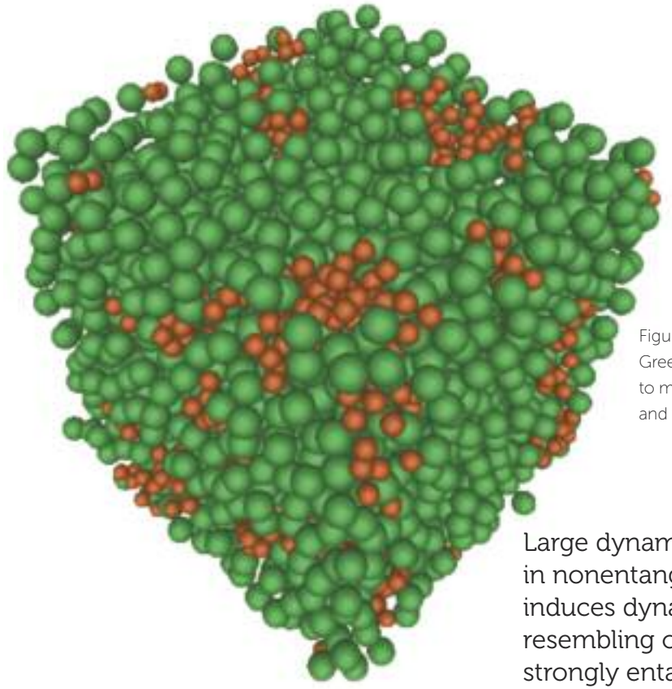

Figure 1. Snapshot of a simulation cell. Green and orange spheres correspond to monomers of, respectively, the slow and fast components of the blend.

Large dynamic asymmetry in nonentangled polymer blends induces dynamic features resembling observations in strongly entangled homopolymers.

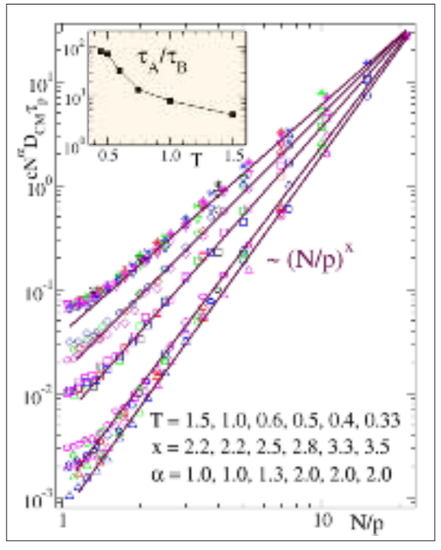


Figure 2. Main panel: For the fast B-component in the AB-blend, scaling of the relaxation times of the chain normal modes, $\tau_p$, versus their wavelength N/p. Inset: Temperature (T) dependence for the ratio of the structural relaxation times of the slow A- and fast- B components, which quantifies dynamic asymmetry. N is the number of monomers per chain. $D_{CM}$ is the diffusivity of the chain center-of-mass. Each symbol code corresponds to a different temperature (see legend), and each color code to a different N. Lines describe power law behavior ~ $(N/p)^x$. The exponent changes from standard Rouse behavior, x ≈ 2, at high T (weak dynamic asymmetry) to anomalous behavior, x ≈ 3.5, at low T (strong asymmetry).

We suggest a more general frame, beyond reptation-based models, for chain relaxation features usually associated to entanglement effects.

# Dynamic arrest in polymer melts: competition between packing and intramolecular barriers

Marco Bernabei, Angel J. Moreno and Juan Colmenero
Physical Review Letters 101, 255701 (2008)

**By means of simulations, we investigate the role of intramolecular barriers on the glass transition of polymers. An analysis within the framework of the Mode Coupling Theory reveals a fundamental difference between the nature of the glass transition in polymers and in simple glass-formers.**

**Since they do not easily crystallize,** polymers are probably the most extensively studied systems in relation with the glass transition phenomenon. Having said this, their macromolecular character, and in particular chain connectivity, must not be forgotten. Another particular ingredient of polymers is the presence of intramolecular barriers. Thus, they are responsible of partial or total crystallization, and can enhance reptation effects. Semiflexible polymer models are of great interest, since they can be applied to many important biopolymers. Thus, an understandig of the structural, dynamical and rheological properties of semiflexible polymers is of fundamental as well as of practical interest. In this work we present computer simulations of a simple bead-spring model for polymer melts with intramolecular barriers, covering the range from fully-flexible to stiff chains (Figure 1). By systematically tuning the strength of the barriers, we investigate their role on the glass transition. Dynamic observables are analyzed within the framework of the Mode Coupling Theory (MCT) of the glass transition. Critical nonergodicity parameters, critical temperatures and dynamic exponents are obtained from consistent fits of simulation data to MCT asymptotic laws.

The so-obtained MCT λ-exponent increases from standard values, characteristic of simple glass-formers, for fully-flexible chains, to values close to the upper limit λ = 1 for stiff chains (see Figure 2). In analogy with systems exhibiting higher-order MCT transitions, we suggest that the observed large λ–values arise from the interplay between two distinct mechanisms for dynamic arrest: general packing effects and polymer-specific intramolecular barriers. With this, the systematic study of the effect of intramolecular barriers presented here establishes a fundamental difference between the nature of the glass transition in polymers and in simple glass-formers.

The study presented here establishes a fundamental difference between the nature of the glass transition in polymers and in simple glass-formers.

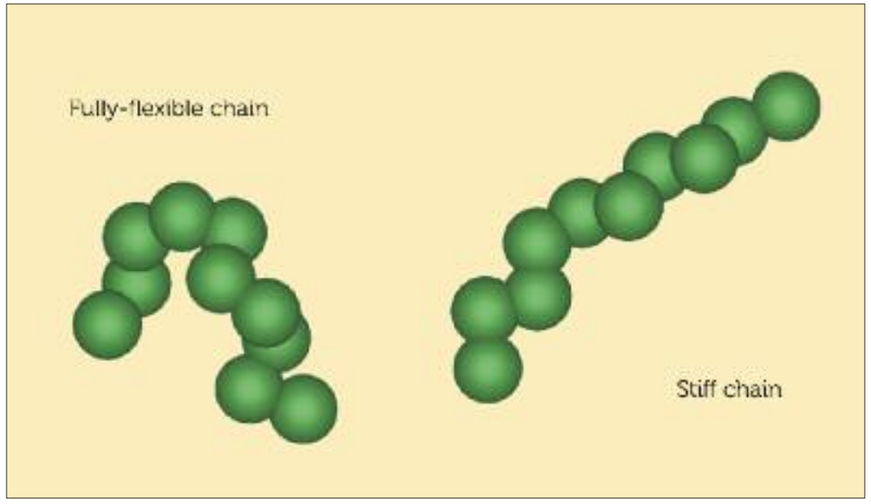


Figure 1. Typical conformations of fully-flexible and stiff simulated chains.

A higher-order MCT scenario arises from the interplay between two distinct mechanisms for dynamic arrest: general packing effects and polymer-specific intramolecular barriers.

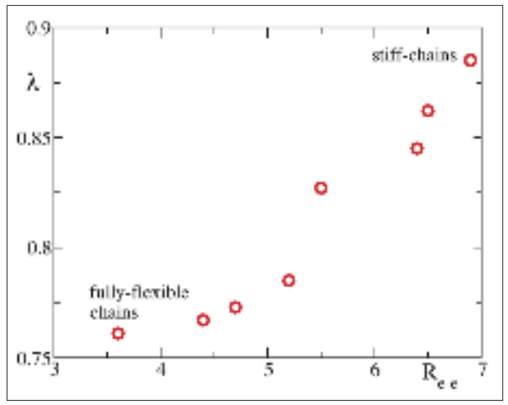


Figure 2. Variation of the MCT λ-exponent with the average chain end-to-end radius, which quantifies chain stiffness.

# Controlling the near-field oscillations of loaded plasmonic nanoantennas

M. Schnell, A. Garcia-Etxarri, A. J. Huber, K. Crozier, J. Aizpurua and R. Hillenbrand
Nature Photon 3, 287-291 (2009)

**An innovative method for controlling light on the nanoscale by adopting tuning concepts from radio-frequency technology is presented. The method opens the door for targeted design of antenna-based applications including highly sensitive biosensors and extremely fast photo-detectors for biomedical diagnostics and information processing.**

**An antenna is a device designed to transmit** or receive electromagnetic waves. Radio frequency antennas find wide use in systems such as radio and television broadcasting, point-to-point radio communication, wireless LAN, radar, and space exploration. In turn, an optical antenna is a device which acts as an effective receiver and transmitter of visible or infrared light. It has the ability to concentrate (focus) light to tiny spots of nanometer-scale dimensions, which is several orders of magnitude smaller than what conventional lenses can achieve. Tiny objects such as molecules or semiconductors that are placed into these so-called "hot spots" of the antenna can efficiently interact with light. Therefore optical antennas boost single molecule spectroscopy or signal-to-noise in detector applications.

In this study, the researchers studied a special type of infrared antennas, featuring a very narrow gap at the center. These so called gap-antennas generate a very intense "hot spot" inside the gap, allowing for highly efficient nano-focusing of light. To study how the presence of matter inside the gap (the "load") affects the antenna behavior, the researchers fabricated small metal bridges inside the gap (Figure b). They mapped the near-field oscillations of the different antennas with a modified version of the scattering-type near-field microscope  that the Max Planck and nanoGUNE researchers had pioneered over the last decade. For this work, they chose dielectric tips and operated in transmission mode, allowing for imaging local antenna fields in details as small as 50 nm without disturbing the antenna. By monitoring the near-field oscillations of the different antennas with this novel near-field microscope, it is possible to directly visualize how matter inside the gap affects the antenna response. The effect could find interesting applications for tuning of optical antennas.

Bridging the gap in nanoantennas.

The nanooptics group from DIPC fully confirmed and helped to understand the experimental results by means of full electrodynamic calculations. The calculated maps of the antenna fields are in good agreement with the experimentally observed images. The simulations add deep insights into the dependence of the antenna modes on the bridging, thus confirming the validity and robustness of the "loading" concept to manipulate and control nanoscale local fields in optics.

Furthermore, the researchers applied the well developed radio–frequency antenna design concepts to visible and infrared frequencies, and explained the behavior of the loaded antennas within the framework of optical circuit theory. A simple circuit model showed remarkable agreement with the results of the numerical calculations of the optical resonances. By extending circuit theory to visible and infrared frequencies, the design of novel photonic devices and detectors will become more efficient. This bridges the gap between these two disciplines.

With this work, the researches provide first experimental evidence that the local antenna fields can be controlled by gap-loading. This opens the door for designing near-field patterns in the nanoscale by load manipulation, without the need to change antenna length, which could be highly valuable for the development of compact and integrated nanophotonic devices.

Nanoantenna loading allows for near-field control in the nanoscale.

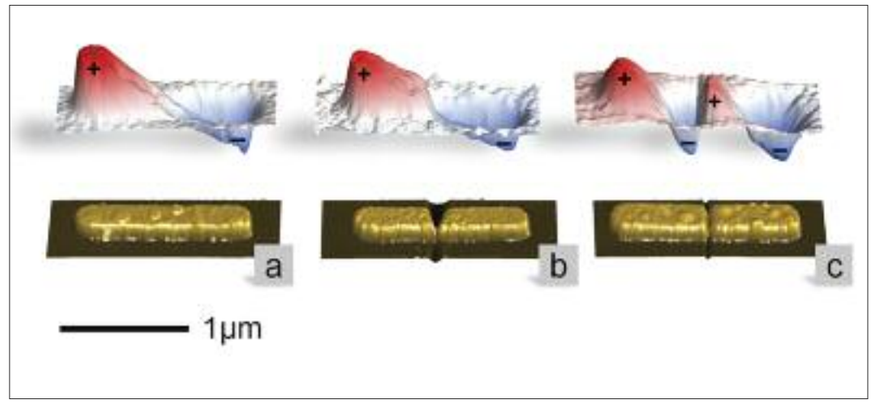


Near-field microscope images of loaded infrared antennas. The bottom line depicts the topography, whereas the upper line plots the scanned near-field images. Figure a) shows a metal nanorod that can be considered the most simple dipole antenna. The near-field image clearly shows the dipolar oscillation mode with positive fields in red and negative fields in blue color. By introducing a narrow gap at the center of the nanorod thus altering the "antenna load" (Figure c), two dipolar-like modes are obtained. When the gap is connected with a small metal bridge (Figure b), the dipole oscillation mode of Figure a) can be restored as the near-field image clearly reveals.

# Novel structures and superconductivity of silane under pressure

Miguel Martinez-Canales, Artem R. Oganov, Yanming Ma, Yan Yan,
Andriy Lyakhov, and Aitor Bergara
Physical Review Letters 102, 087005-8 (2009)

**Understanding the complex behavior** of the simplest element remains a hot topic in condensed matter physics. Soon after the BCS theory for superconductivity was established, Neil W. Ashcroft realized that a very high Tc was plausible. Nevertheless, 70 years after metallic hydrogen was predicted, it still is an elusive goal of physics. Main arguments leading to a high Tc superconducting hydrogen are its light mass and the expected strong electron-ion interactions. It has been recently suggested that these arguments should also hold for metallic alloys with a high hydrogen content. The heavier elements in these alloys are expected to *"chemical precompress"* the hydrogen and, therefore, lower the pressure threshold required for the metallization. Group IVa hydrides have been pointed as obvious candidates. Between them, silane has been subject of most theoretical and experimental research so far, which has prompted us to thoroughly analyze compressed silane using *ab initio* methods coupled with evolutionary structure prediction algorithms.

According to our calculations (Figure 1), in the lower pressure range, between 10 and 25 GPa, the most stable structure is the molecular *P21/c*. At 25 GPa we have a pressure-induced structural transition to a phase of symmetry *Fdd*2. From the electronic point of view, the band gap has a drastic reduction and in the *Fdd*2 structure the gap decreases from 2 eV to 1 eV in its pressure range of stability. The presence of such small gap explains the strong changes in the optical properties: silane becomes completely black and opaque in this pressure range.

As seen in Figure 1, at 55 GPa there are four competitive structures (*Fdd*2, *I*41/*amd*, *P*2/*c* and *I*41/*a*) with the same enthalpy. The latter three structures share the presence of Si-H-Si chains and are radically different from the semimolecular *Fdd*2 (Figure 2). Actually, above 55 GPa the *Fdd*2 structure undergoes a significant change, as the second neighbors of H atoms are no longer H but Si and, therefore, increasing the pressure will not just compress the structure but favors the formation of polymeric Si-H-Si chains and makes unavoidable the transition to the also insulating *I*41/*a* phase, which remains stable up to 220 GPa.

In the high pressure range (Figure 1), insulating tetragonal *I*41/*a* eventually gives way to a new metallic structure of symmetry *Pbcn* (Figure 2), marking the threshold at which, according to our calculations, silane adopts a metallic ground state. The *Pbcn* structure shows an interlayer alloy-like atomic arrangement, with slightly displaced almost square Si layers and H atoms lying in the interlayer spaces of the structure. Given the layered character of the *Pbcn* structure and the high concentration of H atoms, it is likely that this structure might display electronic similarities to pure metallic hydrogen not seen in previously proposed structures. Interestingly, we have performed electron-phonon calculations at 190 GPa and according to the Allen-Dynes approximation, metallic *Pbcn* silane would become a superconductor with a *Tc* of 16.5 K.

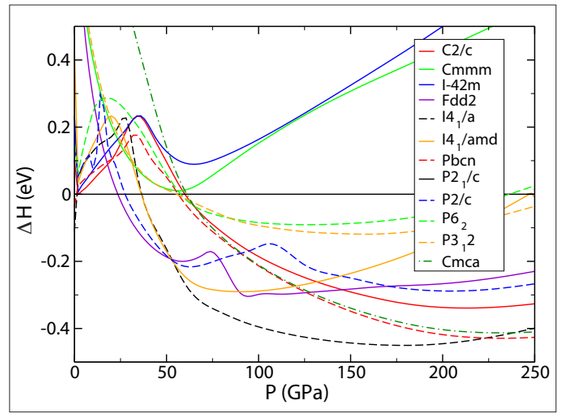


Figure 1. Enthalpies of the most favorable structures. Interestingly, at 55 GPa four competing structures have the same enthalpy and silane changes from intermediate between molecular and polymeric to a fully polymeric phase. The experimentally suggested $P6_3$ structure lies always at least 1 eV above the reference *P*21/*c* structure.

Heavier elements in hydrogen rich alloys chemically precompress hydrogen and lower the threshold pressure required for the metallization.

According to our calculations, silane might become a good superconductor above 200 GPa.

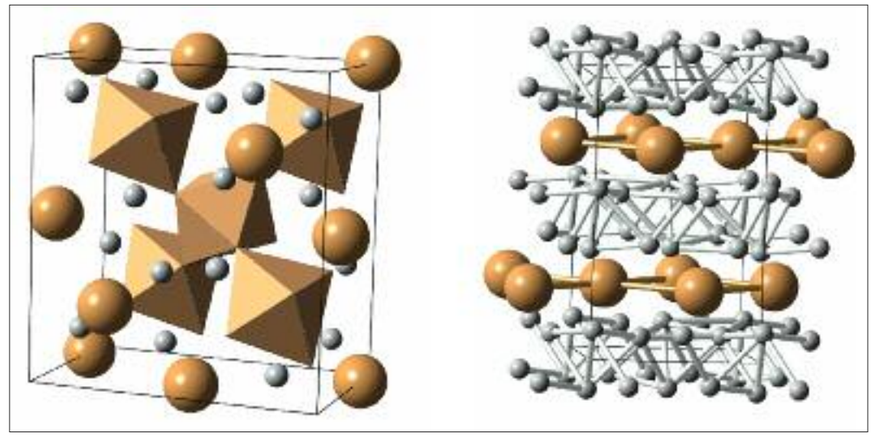

Figure 2. Novel structures of silane. Large atoms depict Si, while small atoms represent H. Left: *Fdd*2 silane, stable between 25 and 55 GPa. Right: *Pbcn* silane, which is metallic, superconducting and favored above 220 GPa.

# Reduction of the superconducting gap in ultrathin Pb islands

Christophe Brun, I-Po Hong, François Patthey, I. Yu. Sklyadneva,
R. Heid, P.M. Echenique, K.P. Bohnen, E.V. Chulkov, and Wolf-Dieter Schneider
Physical Review Letters 102, 207002 (2009)

**The fundamental question of how** the superconducting properties of a material are modified when its thickness is reduced down to a few atomic monolayersis of special relevance for possible technological applications in superconducting nanodevices. The early model of Blatt and Thompson predicted an increase of the critical temperature $T_c$ above the bulk value with decreasing film thickness, together with $T_c$ oscillations due to quantum size effects. However, if proper boundary conditions allowing for spill-out of the electronic wave functions in thin films are taken into account, a decreasing $T_c$ with decreasing film thickness was predicted. In this Letter, we report  in situ layer-dependent STS measurements of the energy gap of ultrahigh-vacuum grown single-crystal Pb/Si(111)-7x7 and Pb-(√3x√3/)Si(111) islands in the thickness range of 5 to 60 monolayers (ML). Also employing layer-dependent \emph{ab initio} density functional calculations for free-standing Pb films, we find for thin layers a similar behavior of $T_c$, caused by a thickness dependent decrease of the electron-phonon coupling.

Figure 1 shows an STM image of a flat-top Pb island extending over two Si terraces separated by a single Si(111) step. The island mainly consists of an 8 ML thick Pb area with respect to the Si surface, as determined from the apparent height in the STM topograph. The island thickness includes the ≈1ML wetting layer. The inset shows a magnified view of the Pb surface lattice with atomic resolution.

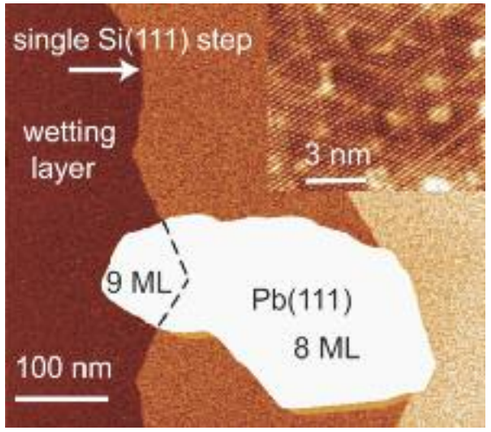


Figure 1. STM image of a flat-top Pb(111) single-crystal island grown on Si(111)-7x7. The island extends over two Si terraces. Island thickness includes the wetting layer. $V_{bias}$ = -1.0 V, I = 100 pA. The inset shows a magnified view, revealing the Pb lattice with atomic resolution ($V_{bias}$ = 20 mV, I = 1 nA).

For all thicknesses studied, the largest contribution to the e-ph coupling originates from electronic states of $p_z$ symmetry: both surface- and bulk-like $p_z$ states contribute to **λ**. The states of in-plain symmetry, $p_x$ and $p_y$, play a minor role in the e-ph coupling. The e-ph coupling matrix elements do not affect qualitatively the phonon DOS F(**ω**): the calculated Eliashberg function **α**2F(**ω**) shows the same peak structure as the phonon DOS F(**ω**), all phonon modes contribute to **λ**. This result is in good agreement with the absence of significant changes in the measured phonon energies in the dI/dV spectra upon thickness reduction. Fig. 2 shows that the theoretical $T_c$ are in fairly good agreement with the trend observed from the present STS data. The calculated $T_c$ for the 5, 6 and 7 ML film are larger than those estimated from the measured gap values. This might be ascribed to the larger discrepancy arising at small film thickness between calculated and measured QWS energies, the latter being smaller.

For thin Pb islands on Si(111) the experimentally observed reduction of the superconducting energy gap with decreasing film thickness is consistent with the first principle results of a thickness-dependent e-ph coupling constant **λ**, where close to the ultrathin Pb film limit the variations of the density of states at $E_F$ play a decisive role. Interestingly, both atomically smooth (Pb/Pb-√3x√3/Si) and disordered (Pb/Si-7x7) interfaces yield similar experimental behavior, in agreement with results showing that both systems are in the diffusive limit.

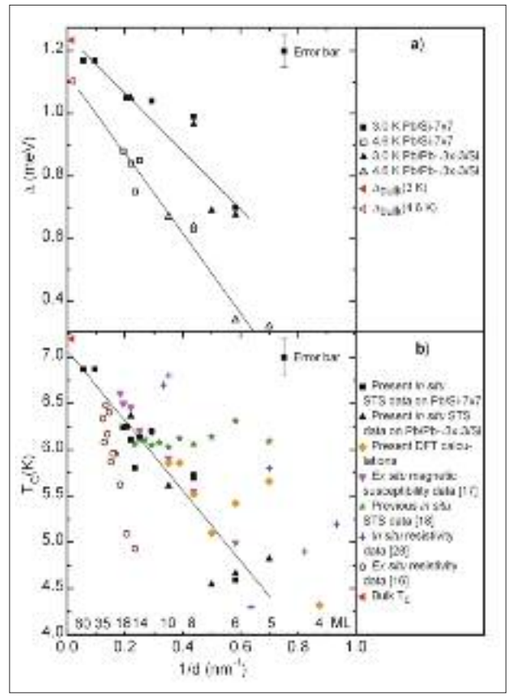


Figure 2. Superconducting energy gap Δ as a function of inverse Pb island thickness 1/d, extracted from BCS fits of dI/dV tunneling spectra, for the crystalline (Pb/Pb-√3x√3/Si) and disordered (Pb/Si-7x7) interface. Continuous lines are guide for the eyes. b) Estimated critical temperature T_c as a function of 1/d, using the bulk $\Delta/T_c$ ratio and assuming BCS temperature dependence of Δ(T), to allow comparison with previously reported results. Continuous line is a fit to the present STS data. For both a) and b) error bars: experimental dispersion and uncertainty in the fit results. All the references indicated can be found in the present publication reference list.

# One-electron model for the electronic response of metal surfaces to sub-femtosecond photoexcitation

A.K. Kazansky and P.M. Echenique
Physical Review Letters 102, 177401 (2009)

**One-dimensional model for analysis of sub-femtosecond streaking experiment with metal surface is suggested. The important features of the system, such as a pseudopotential for electron motion in the metal bulk, an abrupt decrease of the normal to the surface external electromagnetic field in the bulk, a finite value of the mean free path for electrons in the metal, and an action on the ejected electron of the (stationary) screened positive hole in the metal are included in the model. The results obtained in our computations reveal a simple dependence of the delay on the final energy of an electron ejected from the localized state. The results of our computations are in very good agreement with the measurements.**

**Study of the real-time dynamics** of electrons in condensed-matter systems is pertinent for progress in nanotechnology. The electron processes in nano-systems are very fast and their investigation in real time requires application of experimental tools with sub-femtosecond time resolution. Recently, the first experiment [1] with streaking observation of electron dynamics in metal in the sub-femtosecond range was performed. In this experiment, the surface of solid was illuminated by two pulses. The first pulse was a short XUV pulse with the frequency of about 90 eV and duration (FWHM for the field envelope) of about 0.2 fs. Intensity of this pulse was quite low. Another pulse was a relatively strong (power W in 10^9 – 10^10 W/cm^2 range) near-infrared (NIR) laser pulse with the frequency of about 1.5 eV and with the duration of about 10 fs. The energy spectra of the electrons ejected from the localized f-state and delocalized band through the (110) surface of tungsten in the direction normal to this surface were measured. The time delay between the two pulses was varied and the energy spectra of the ejected electrons were monitored as a function of this delay. These energy spectra are the result of steering of the electrons, ejected from the metal by the XUV pulse, by the electric field of the NIR pulse in vacuum. The energy acquired by the ejected electron from the NIR field depends on the time of the electron passage across the metal surface. Thus, with measuring the dependence of the ejected electron energy spectrum on the time delay between the pulses, one can keep track on the process dynamics in the time domain.

The processes triggered by the instantaneous excitation of an electron in a solid are very complicated and a number of various mechanisms can be of paramount importance. First, electrons in the metal are moving in the field of the lattice. This can change the group velocity of the excited electron packet inside the bulk. Second, a localized electron after its ejection leaves in the bulk a positively charged hole which is then screened by the itinerant electrons. Third, the ejected electrons suffer inelastic collisions with electrons of the metal. This determines the depth from which the ejected electrons can reach the surface without inelastic collisions and thus carry direct information on the processes in the bulk. Fourth, the normal component of the laser field decreases in the bulk abruptly to a very small value under the condition of the experiment. This determines the peculiarity of streaking effect in the system considered.

We have formulated a simple and versatile model which allows one to estimate the magnitude of the possible effects and to analyze the influence of the parameters of the system on the output. Our model includes the main ingredients of the short time physics involved in the experiment. Within our model, we have computed the time-delay in the streaking spectra of the electrons ejected from the localized and localized electrons that was measured experimentally. The calculations, despite using a one-dimensional model potential, apply a time-dependent approach and take into account all relevant effects leading to a reasonable agreement with experiment. As a result of our computation, we have obtained for the time delay 85 attoseconds, while the experimental result [1] was at that time rather indefinite: 110±70 as. Later the experiment was repeated and the improved result is very close to our prediction. Worthy to emphasize that this is a unique result of a quantitative measurement of an phenomenon in a solid state with an attosecond experimental setup.

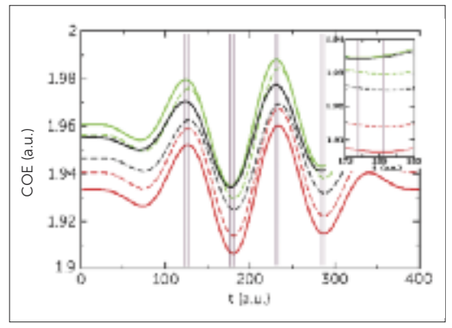


The positions of the center of energy of electron spectra ejected perpendicularly to the W surface are plotted. Solid lines correspond to the result for the total spectra, the red line shows the center of energy for electrons emitted from the delocalized initial state with the final energy E = 2 a.u., the black line corresponds to the same quantity obtained for the case of localized initial state with the final energy E = 2 a.u., and the green line gives the result obtained for the case of the initial local state, but with final energy E = 3 a.u. (The curves are shifted along the energy axis to the same scale.) The dashed lines, black and green, show contributions from the topmost atoms for the two values of final energy given above, and the dashed red line shows the center of energy for the electron ejected from the top of the delocalized band. The computed energy shift is clearly seen in the insert as a difference in position of minima of the curves.

We determine the peculiarity of streaking effect in the system considered.

# Hydrogen-bonding fingerprints in electronic states of two-dimensional supramolecular assemblies

N. Gonzalez-Lakunza, M.E. Cañas-Ventura, P. Ruffieux, R. Rieger, K. Müllen, R. Fasel, A. Arnau
ChemPhysChem, 10, 2943-2946 (2009)

**DFT calculations reveal that the molecular orbital energy shifts observed in STS experiments of 2D assemblies with different hydrogen-bonding patterns originate from modifications in the electrostatic potential energy due to a bipolar charge redistribution in anisotropic triple hydrogen bonds within heteromolecular systems.**

**Chemical bonding** is intimately related to the valence electronic structure, but changes in the local molecular orbital structure due to different hydrogen-bonding environments in bi-dimensional assemblies have not been explored in detail so far. In ref. [1], by comparing distinct hydrogen-bonding configurations for two molecular species, we have provided the spectroscopic fingerprint of such changes, which are explained in terms of charge polarization at the molecular scale induced by anisotropic triple hydrogen bonds.

We have studied the unoccupied electronic states of mono- and bicomponent assemblies of 1,4-bis-(2,4-diamino-1,3,5-triazine)-benzene (BDATB) and 3,4,9,10-perylenetetracarboxylic diimide (PTCDI) on Au(111), by combining low-temperature scanning tunneling spectroscopy experiments and density functional theory based calculations. Homomolecular BDATB and PTCDI assemblies exhibit a twofold frontal hydrogen-bonding configuration, while the heteromolecular BDATB-PTCDI system is stabilized by a threefold frontal hydrogen-bonding array [Fig. 1a)-c)]. It turns out, that when comparing the dI/dV spectra of pure and mixed systems, that is in going from the frontal twofold to the threefold hydrogen-bonding configuration, quite large energy shifts are observed. BDATB peaks present an upward shift, whereas PTCDI peaks shift downwards. The origin of these shifts is understood thanks to first-principles DFT calculations of the free-standing molecular layers. We find that the electrostatic potential energy around each molecular species is clearly modified due to an effective bipolar charge redistribution induced in the anisotropic tripe hydrogen bonds within the heteromolecular systems. In other words, in going from the pure systems to the mixture the electrostatic potential at BDATB gets more repulsive and the potential at PTCDI gets more attractive, finally leading to the observed upward and downward energy shifts.

STS signatures of complementary H-bonds formation are shown.

Our results do not only provide detailed new insight into the hydrogen-bonding interactions driving the self-assembly, but also provide the perspective to control and design the electronic properties of hydrogen-bonded supramolecular architectures.

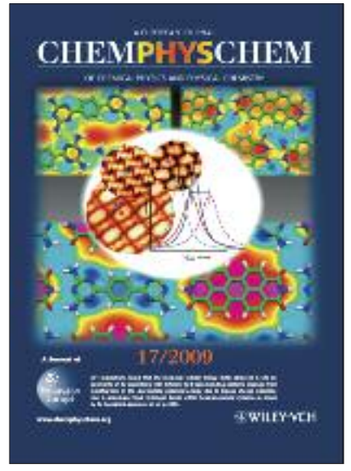


Inside cover ChemPhysChem: Ref. [1] featured in the inside cover of ChemPhysChem 10th volume. The picture in the center shows schematically the observed energy shifts for STS spectra taken on different molecules, and corresponding experimental STM images. The colored graphs in the background correspond to the electrostatic potential energy distribution depicting its modification in going from the pure systems to the mixed system.

Local polarization at the molecular level explain the observed energy shifts.

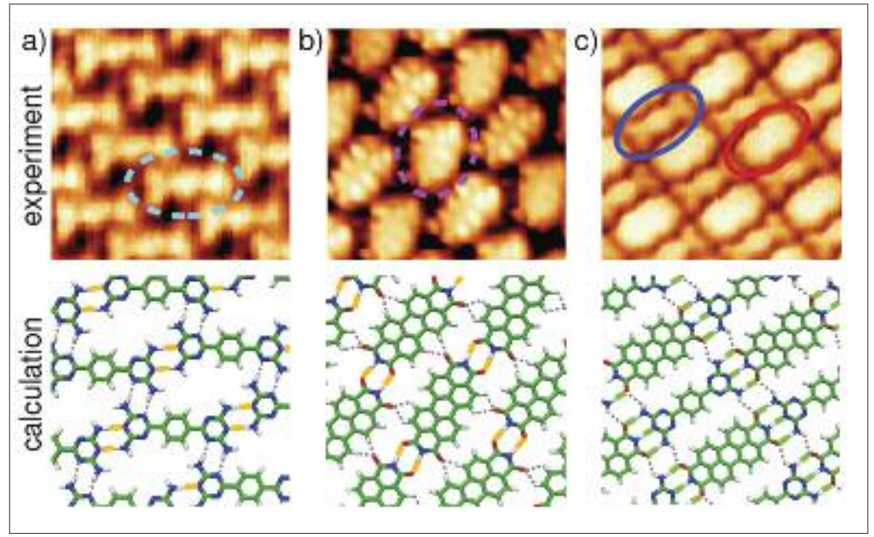


Figure 1. a)-c) STM images from mono- (pure) and bicomponent (mixture) supramolecular self-assemblies on Au(111): a) pure BDATB (1.6 V, 0.03 nA), b) pure PTCDI (-1.7 V, 0.10 nA) and c) BDATB-PTCDI binary mixture (-0.3 V, 0.10 nA). The corresponding bottom panels show the calculated relaxed structures of each periodic system, which illustrate the twofold frontal hydrogen-bonding configuration (marked in yellow) of the monocomponent systems adn the threefold frontal hydrogen-bonding pattern of the mixture (marked in green).

# The pathways of micelle formation

Reidar Lund, Lutz. Willner, Michael Monkenbusch, Pierre Panine,
Theyencheri Narayanan, Juan Colmenero and Dieter Richter
Physical Review Letters, 102, 188301 (2009)

**For the first time, the spontaneous self-assembly of micelles are captured using small angle x-ray scattering techniques with a time resolution in the millisecond range. Detailed modelling shows that the data can be satisfactorily described using a rather simple nucleation and growth model where only one chain can be added at time.**

**In material science and physical chemistry,** self-assembly is an important route for manipulation and control for a rational design of nanostructures. Synthetic amphiphilic block copolymers belong to the family of self-assembling systems which, apart from the spontaneous self-assembly property, exhibits tuneablity via control over block composition, molecular weight and cosolvents. In order to fully understand and exploit the properties of self-assembled structures, the pathways of their formation need to be understood. So far, such a study has been exceedingly difficult if not impossible because of the lack of experimental techniques that are able to capture and resolve the early stage of this rapid process.

Here we have taken advantage of advances in modern synchrotron radiation instrumentation and for the first time been able to capture and describe how self-assembly of amphiphilic block copolymers takes place in real time using the ID02 beamline at ESRF. Using block copolymers that are molecularly dissolved in a organic polar solvent, micellization can be induced by simply adding water. This process has been observed experimentally using the set-up illustrated in Figure 1, where a stopped flow apparatus is used to assure rapid mixing of the two components in a millisecond time scale. The reaction itself is monitored directly using fast X-ray shots with some millisecond time resolution that allowed the observation of the birth and growth of the micellar aggregates in time. The obtained scattering curves contain relevant structural characteristics of the micelles, such as sizes, volumes and density profiles.

The observed behavior can be quantitatively reproduced using a kinetic model involving insertion and expulsion of single block polymer chains (unimers) by combining classical nucleation and growth theory with the thermodynamic expression expected for block copolymers. It was assumed that only single molecules (unimers) can be taken up for each cluster at a time. As seen in the simultaneous fits in Figure 2 a), the model agrees very well with the experimentally observed growth. In the beginning a very fast initial nucleation, or primary micellization, that consumes all the unimers can be observed. The final stage of the micellization is governed by unimer exchange following a type of ripening mechanism where small micelles slowly dissolve to provide further unimers and the larger ones gradually grow. This goes on until the micelles approach the shallow minimum of the equilibrium size and the distribution narrows to reflect the thermodynamic equilibrium. This scenario is summarized schematically in Figure 2 b).

The excellent agreement with this model strongly suggests that the most effective way for micelle formation is simple addition of unimers from a homogeneous solution. This insight gives novel and valuable information of not only the formation and kinetic pathways of these structures but also the stability and lifetime of metastable nano-particles. This knowledge may be utilized for facile predictive design and manipulation of nano-structures in e.g. medicine or material science.

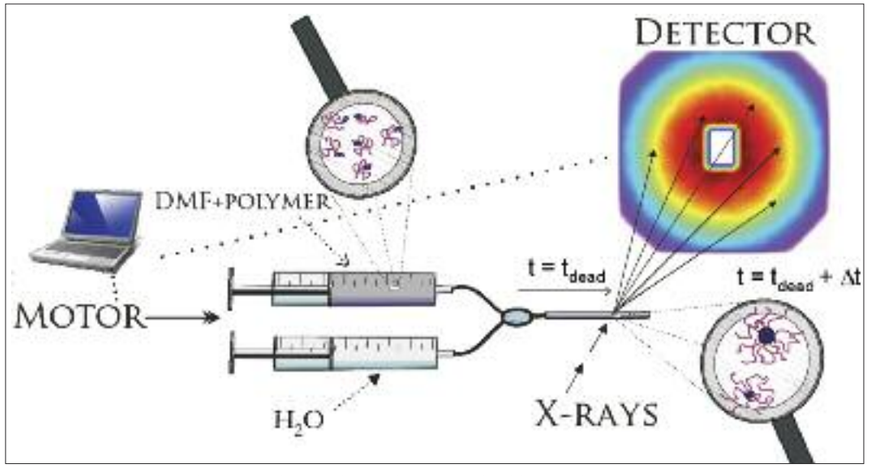


Figure 1. Experimental set-up: The stopped flow set-up consists of two motorized syringes containing the reservoirs with polymer solution and water respectively. Equal amounts of the solution are mixed and then transferred to the observation capillary within a few milliseconds- thereafter the growth is detected by x-ray pulses.

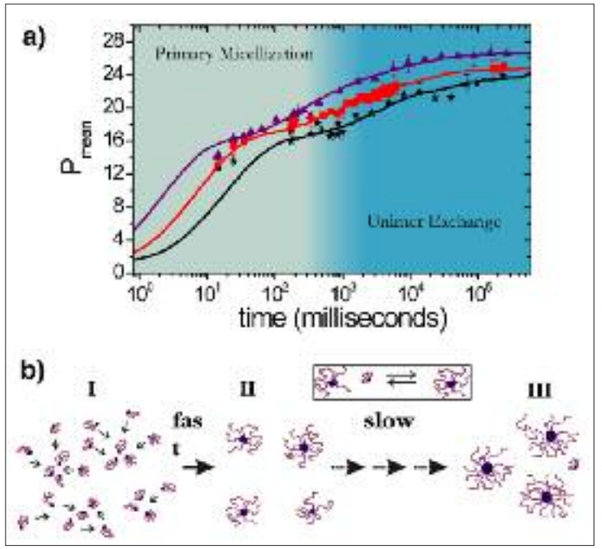


Figure 2. (a) Time evolution of the mean aggregation number of micelles (Pmean) for different concentrations of the block copolymer. Continuous lines represent fits to the nucleation and growth model. (b) Schematic representation of the micellization process involving a fast nucleation in which the unimer concentration is depleted and a slow growth to micelle/unimer.

Micelles seem to grow in a stepwise fashion where only one molecule is inserted or removed at a time.

# Quantum oscillations in coupled two-dimensional electron systems

S. Mathias, S. V. Eremeev, E.V. Chulkov, M. Aeschlimann, and M. Bauer
Physical Review Letters 103, 0268 02 (2009)

**Two prominent examples of electronic systems** with reduced dimensionality are Shockley-type surface (SS) states of the (111) oriented noble metal surfaces and quantum-well (QW) states in ultrathin metallic films. The former are states which are restricted to the outermost atomic surface layers and therefore represent an almost ideal example for two-dimensional electron systems. QW states evolve by the confinement of electrons in ultrathin metal films. QW states arise as the standing electron waves supported by the film and many properties depend critically on the film thickness. These properties show a clear oscillatory dependence on the film thickness (quantum oscillations). We show that such a quantum oscillatory behaviour can efficiently be transferred between two coupled two-dimensional electron systems. Experimentally and from microscopic calculations we have studied the electron-phonon (e-ph) coupling parameter $\lambda$ of the Ag(111) SS band as modified by the thickness of a supporting silver QW. By means of photoelectron spectroscopy we have identified clear oscillations in $\lambda$ as a function of QW thickness. Our microscopic model calculations quantitatively reproduce these experimental findings.

In Figure 1 we show experimental and theoretical $\lambda$ values of the SS state as a function of the thickness of the silver QW between 15 monolayers (ML) and 40 ML. The variations in $\lambda$ of both data sets follow a clear oscillatory behavior. It exhibits an amplitude of ~ 0.02 and an oscillation period of about 10-12 ML. The slightly varying thickness scale between experiment and theory is due to uncertainties in the determination of the film thickness in the experiment. The overall lower values of the theoretical data (~0.1) were expected, since the calculations do not include the constant background of phonon mediated scattering processes from the Cu substrate as well as from defects scattering contribution to the total linewidth. As mentioned above, oscillations in distinct properties of a QW are a rather common behavior arising from the quantization of the electron spectrum in the QW. Our results provide for the first time evidence that such a quantum-oscillatory behaviour can efficiently be transferred to another low-dimensional electronic system that is coupled to the QW. Below we identify the relevant peculiarities which are responsible for this transfer process.

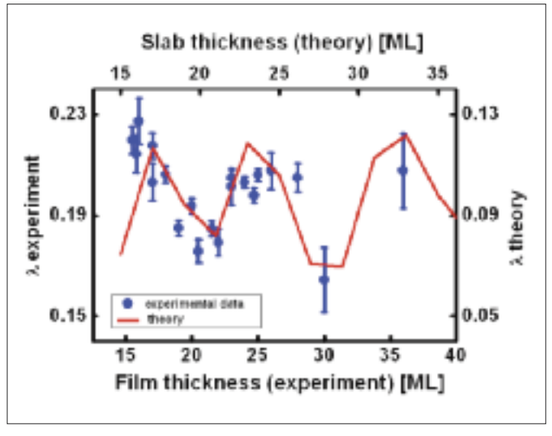


Figure 1. Electron phonon coupling parameter for the SS state as a function of Ag film thickness. Blue dots show the experimental data, the red line the theoretical data.

Figure 2 displays results from a calculation of apartial $\lambda$ of the surface state ($\lambda_{gap\text{-}QWS}$) which considers exclusively QW states in the energy regime of the Cu(111) substrate band gap (below 850 meV binding energy). At distinct film thicknesses an additional QW state moves into resonance with the Cu band gap and, hence, increases the number of QW states, which affect $\lambda_{gap\text{-}QWS}$, by one. The appearance of this additional QW state within the band gap is equivalent to a sudden localization of the QW wave-function in the Ag-film. Such localization takes place for instance at a slab thickness of 22 ML and obviously contributes considerably to the amplitude of the second oscillation maximum of $\lambda_{gap\text{-}QWS}$. The magnitude of $\lambda_{gap\text{-}QWS}$ is, however, by far too small to explain the total amplitude of $\lambda_{SS}$ and accounts for only 10% of the observed experimental value. The overlap of the SS wave function with QW states outside of the Cu(111) band gap accounts for the remaining 90% of the amplitude. The latter, the sum over oscillations of all partial contributions, is obviously a crucial factor responsible for the pronounced oscillations in $\lambda_{SS}$. However, these oscillations cannot be explained by a simple overlap effect. The localization of the SS state wave-function at the surface of the quantum-well is essential ingredient for the observed oscillatory behavior. Another significant ingredient is the gradient of the one-electron potential which enhances the oscillation amplitude of $\lambda_{SS}$.

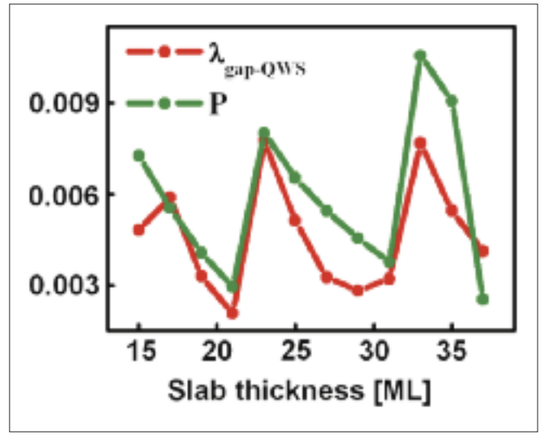


Figure 2. Partial $\lambda$ to the electron phonon coupling parameter of the SS state from the QW states localized in the Cu(111) band gap as a function of film thickness and overlap P of corresponding wave functions.

Our microscopic model calculations quantitatively reproduce these experimental findings.

# Passing current through touching molecules

G. Schull, T. Frederiksen, M. Brandbyge, and R. Berndt
Physical Review Letters 130, 206803 (2009)
Paper selected for "Editor's Suggestion" and American Physical Society's "Physical Review Focus"

**The charge flow from a single $C_{60}$ molecule to another one has been probed. A scanning tunneling microscope (STM) was used to first pick up a single $C_{60}$ molecule with the tip and thereafter to approach it to a second molecule with atomic-scale precision. This novel method allows for detailed studies of intermolecular charge transport, which is crucial for the realization of efficient electronic devices, sensors, and solar cells based on molecular materials.**

**The performance of modern electronics** increases steadily on a fast pace thanks to the ongoing miniaturization of the components. However, severe problems arise due to quantum-mechanical phenomena when conventional structures are simply made smaller and reach the nanometer scale. Therefore current research focuses on the so-called bottom-up approach: the engineering of functional structures with the smallest possible building blocks, namely single atoms and molecules. These efforts have resulted in a detailed insight into the transport properties of individual nanoscopic objects. A critical issue is now to understand and control the charge transport from one molecule to another one.

In this work the intermolecular charge transport through a $C_{60}$-$C_{60}$ bridge was investigated for the first time. In order to realize this setup a technique to transfer a $C_{60}$ molecule to the tip of an STM was devised. Examples of images acquired before and after the transfer of the molecule to the tip is shown in Figure 1. The molecular orientation could be inferred via adatoms deposited on clean areas of the metal substrate. Hereafter the $C_{60}$-functionalized tip was approached to a second molecule with a precision of a few picometers. During this controlled approach the researchers measured the electrical current that flows between the two molecules, which depends critically on the distance between the molecules. Ultimately, the molecules touch each other and the current attains its maximum value.

The investigation revealed that the electrical current does not flow easily between the two touching $C_{60}$ molecules - the conductance is 100 times smaller than for a single molecule. This finding is interesting for future devices with closely packed molecules as it indicates that leakage currents between neighboring circuits will be controllable.

The experimental findings are strongly supported by first-principles transport simulations carried out at the DIPC. These calculations reproduce the experimental results and identifies the role of the intermolecular link in the conductance of the $C_{60}$-$C_{60}$ bridge (Figure 2). The theory further gives access to the distance-dependent nature of the electrical current and predict the evolution of the transport properties for longer chains of suspended $C_{60}$ molecules.

The extreme precision of manipulation and control of single molecules presented in this work open up a new route for exploring other promising molecules to address the influence of the molecule-molecule interactions on intermolecular charge transport. The deeper understanding of this current is an essential step towards novel molecular nanoelectronics.

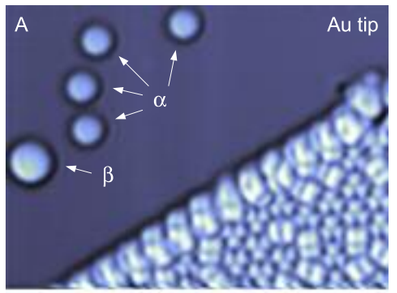


STM images of Au(111) partially covered with C60 molecules (lower right) obtained with (A) a metal tip and (B) a C60-tip over the same area. Gold adatoms (α) and a small gold cluster (β) of two or three atoms are discernable. After imaging with the $C_{60}$-tip it was used to make contact to another $C_{60}$ molecule in order to study the conductance of a $C_{60}$-$C_{60}$ bridge.

Understanding intermolecular charge transport is essential towards novel molecular nanoelectronics.


Image published on the cover of *Physical Review Letters*

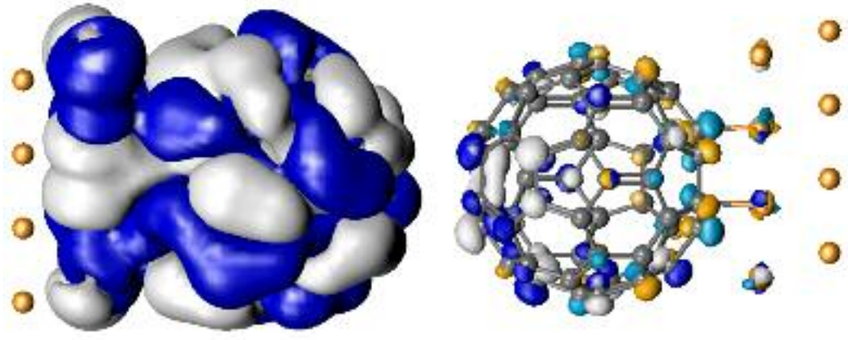

Electron current through two $C_{60}$ molecules contacted with metal electrodes. The isosurface of the electron wave (incoming from the left) extends with large amplitude over the first $C_{60}$ molecule but is reflected at the interface between the two $C_{60}$ cages. The strongly attenuated outgoing wave (to the right) illustrates that the low transmission probability (and correspondingly the relatively low conductance) of the $C_{60}$-$C_{60}$ bridge is due to the intermolecular link.

# Angle-resolved photoemission study of the graphite intercalation compound KC8: a key to graphene

A. Grüneis, C. Attaccalite, A. Rubio, D.V. Vyalikh,
S.L. Molodtsov, J. Fink, R. Follath, W. Eberhardt, B. Büchner, and T. Pichler
Physical Review B 80, 075431 (2009)

**Idealized graphene is a two-dimensional sheet of carbon. The electrons in graphene behave like massless Dirac particles that appear in the electronic band structure as gapless excitations with a linear dispersion—the "Dirac cone." However, in real life, graphene is never perfectly flat and may interact with the substrate that supports it, which significantly alter graphene's electronic properties. Invariably, these effects open a gap that limits the observation of relativistic physics in graphene.**

**Every week there are numerous papers** explaining the exotic features of graphene, a single layer of carbon atoms arranged in a honeycomb lattice. Due to the honeycomb lattice, electrons in graphene behave as massless particles. In ideal, freestanding graphene, electrons can move through the crystal without scattering with carbon atoms. This is very much the way that light propagates (with a velocity that is only 1/300 of the speed of light). Therefore electrons in graphene are described by the Dirac equation – indeed this is something very unique in condensed matter physics. Unfortunately this ideal view of graphene contrasts with experimental evidences where coupling with the substrate or to adjacent graphene layers spoils the massless Dirac Fermion behaviour predicted from the theory. In this case the substrate interaction causes the electronic structure to open up a gap and the electrons to acquire a finite mass. Then they are no longer described by the Dirac equation.

In this article researchers from the IFW in Dresden, Germany, and collaborators from Austria and Spain observe the full Dirac cone dispersion, expected for isolated graphene, in an intercalated graphite compound KC8 using angle resolved photoemission spectroscopy. The potassium ions move in between individual graphene sheets (this process is also known as intercalation) thereby separating adjacent graphene layers apart and cancelling their interaction. The KC8 crystal consists of individual graphene sheets separated by layers of potassium. Combining angle-resolved photoemission spectroscopy measured at the BESSY synchrotron in Berlin and theoretical calculations from DIPC and the European Theoretical Spectroscopy Facility, they unravelled the full experimental Dirac cone of electrons in graphene revealing an anisotropic linear dispersion in all directions, the same way how light propagates (see Figure). It turns out that there is a complete charge transfer from potassium to the graphene layers but there is no Coulomb interaction between the layers. This preserves the Dirac cone dispersion for both the valence and conduction bands, though the doping shifts the Dirac point away from the chemical potential (differently from what is expected for pristine graphene). This allowed them to measure not only the valence bands but also the conduction bands of graphene for a large energy range, not reachable in single layer graphene. State-of-the art electronic structure calculations including electron-electron interactions within the graphene sheets needs to be taken into account to get excellent agreement with experimental. These results provide crucial input to study the electronic and transport properties of isolated graphene, which has hitherto been difficult due to substrate effects.

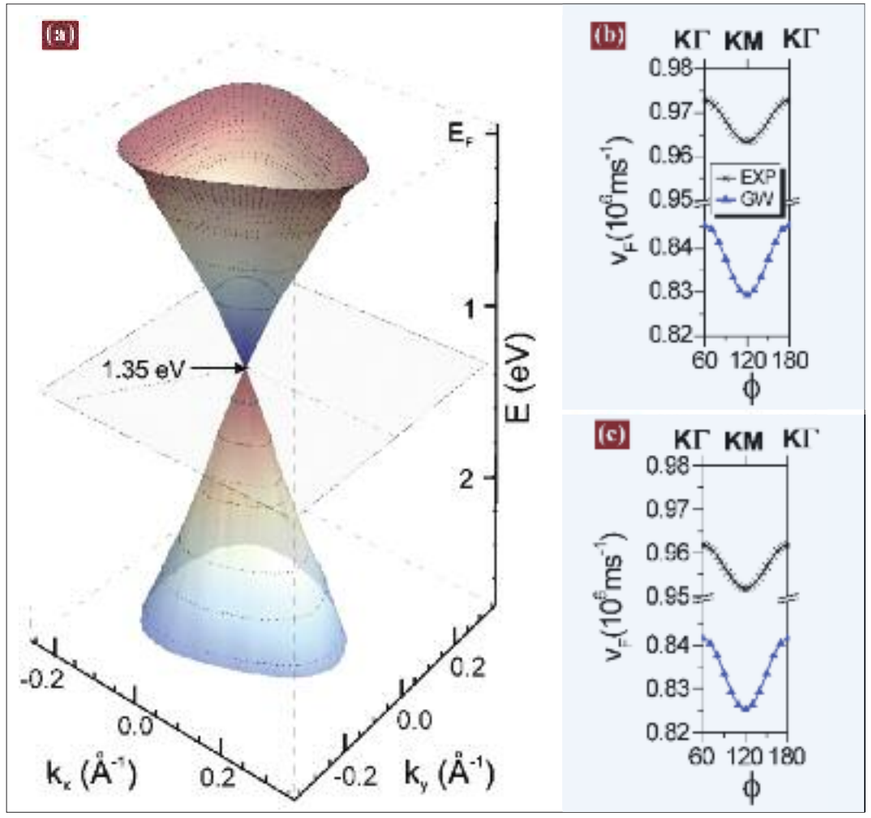


Figure 1. (a) Experimental Dirac cone from the observed photoemission intensity maxima (denoted as dots). Measured and calculated (GW) values of vF for (b) electrons and (c) holes around the Dirac point.

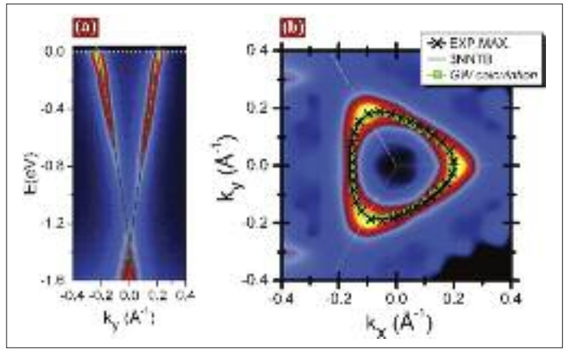


Figure 2. (a) ARPES scan measured close to the ky direction along with the bare-band dispersion (black) and the GW calculation for rigidly doped graphene (green).
(b) Symmetrized equi–energy contour for E=0.24 eV and maxima (crosses) along with a tight-binding fit and the GW ab-initio calculations.

Dirac cone revealed.

# Acousto-plasmonic hot spots in metallic nano-objects

N. Large, L. Saviot, J. Margueritat, J. Gonzalo,
C.N. Afonso, A. Arbouet, P. Langot, A. Mlayah and J. Aizpurua
Nano Letters 9, 3732 (2009)

We introduce the concept of acousto-plasmonic dynamics of metallic nano-objects. Acousto-plasmonic interactions still present several theoretical challenges to correctly interpret the Raman-Brillouin scattering. Several works have been devoted to the study of shape, size and environment effects on the surface plasmons whereas there are only few studies of their dynamical properties such as coupling mechanisms to the acoustic vibrations.

**We experimentally observe unexpectedly** strong acoustic vibration bands in the Raman scattering of silver nanocolumns (NCIs), usually not found in isolated nano-objects. The frequency and the polarization of this unexpected Raman band allow us to assign it to breathing-like acoustic vibration modes (blue arrow in Figure 2). To understand this "anomalous" Raman scattering, we address a theoretical and experimental study of the interactions between acoustic vibrations (upper part of Figure 1) and surface plasmons (lower part of Figure 1). The modulation of the surface plasmon nearfield (lower part of Figure 1) allows for the interpretation of experimental Raman-Brillouin spectra in these NCIs.

Based on full electromagnetic near-field calculations coupled to the elasticity theory, we introduce a new concept of "acousto-plasmonic hot spots" which arise here because of the indented shape of the NCIs. These hot spots combine both highly localized surface plasmons and strong shape deformation by the acoustic vibrations at specific sites of the nano-objects. In order to investigate this new concept, we integrate the Boundary Element Method for the electromagnetic calculations and the elasticity theory by the means of the RUS method for the vibrational calculations, which allows calculating the modulation of the surface plasmon polarization for these acoustic vibrations.

We show that the interaction between breathing-like acoustic vibrations and surface plasmons at the "acousto-plasmonic hot spots" is strongly enhanced, turning almost silent vibration modes into efficient Raman scatterers. The indentations of the silver NCIs are responsible for the strong localization of the surface plasmon nearfield and its modulation by breathing-like acoustic vibrations (Figure 2). The concepts, the numerical and experimental approaches developed here are not specific to indented NCIs and can be extended to other isolated nano-objects exhibiting strong field localization, dimers and more complex metallic nanostructures combining size, shape and interaction effects.

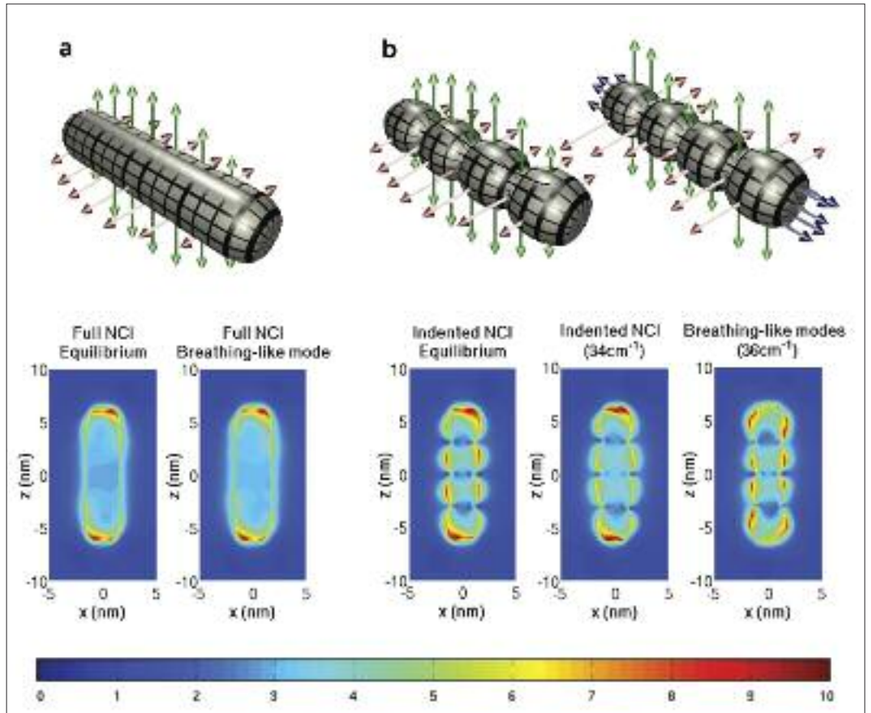


Figure 1. Upper part: Displacement field associated to the breathing-like acoustic vibrations for (a) a full NCI and (b) an indented NCI. Lower part: Nearfield disctribution for (a) a full NCI and (b) an indented NCI at the equilibrium (without vibrations) and deformed by the breathing-like acoustic modes.

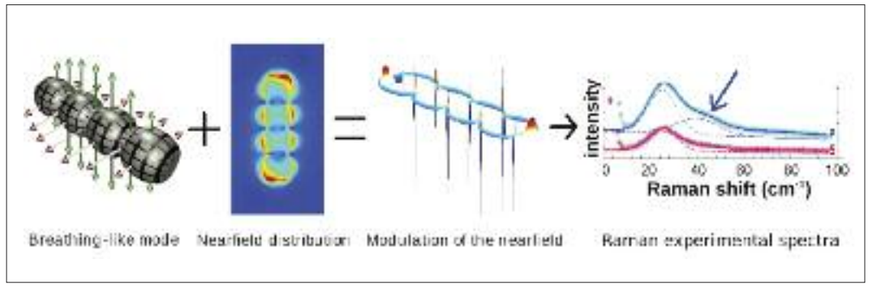


Figure 2: Breathing-like acoustic vibrations modulate the surface plasmon nearfield of a silver indented NCI and induce a relative modulation of the surface plasmon polarization $\delta_{vib}P(r)/P_0(r)$. This modulation is responsible for the activation of the "anomalous" acoustic band (marked with the blue arrow) in the Raman spectrum.

# Supramolecular environment-dependent electronic properties of metal-organic interfaces

Dimas G. de Oteyza, Juan María García-Lastra, Martina Corso, Bryan P. Doyle,
Luca Floreano, Alberto Morgante, Yutaka Wakayama, Angel Rubio and J. Enrique Ortega
Advanced Functional Materials 19, 3567 (2009)

**In this work, we address the changes in the electronic structure of donor-acceptor molecular mixtures with respect to that of the isolated components. The changes arise as a consequence of the modified interactions in the supramolecular layers, whose understanding is crucial for a better control of the self-assembly processes on surfaces.**

**Charge transfer processes** between donor–acceptor complexes and metallic electrodes are at the heart of novel organic optoelectronic devices such as solar cells. In fact, molecular dyads allow the development of new architectures according to a win-win design strategy, thanks to the varied properties offered by organic semiconductors. On the one hand, the optical sensitivity of the photovoltaic cell can be tuned to the environmental light conditions by appropriate choice of the molecular pair. On the other hand, the intermolecular interactions can be trimmed by chemical functionalization of the respective molecules, in order to optimize the molecular coupling in the supramolecular assembly. The bottleneck of this emerging technology is represented by the interface with the supporting metal contact, where the charge signal is extracted. Most studies on interfacial electronic properties, which are crucial factors for charge carrier injection/extraction and thus for the functionality of organic based optoelectronic devices, have been performed on model single-component molecular layers on metals. In spite of the expected key role of nanostructured donor–acceptor systems in future development of organic devices, these have been mostly studied from a structural and only scarcely from an electronic point of view. Here we show that the charge transfer and the chemical properties of metal-organic interfaces based on single component organic layers cannot be naively extrapolated to the new molecular environments of supramolecular architectures, such as donor–acceptor binary assemblies. As a consequence, a detailed atomistic understanding of the hybrid junction between electrode and organic mixture (both from an electronic and structural point of view) is required for a rational design of functional donor–acceptor nanostructures with optimized properties.

Our study focused on binary supramolecular nanostructures on copper (111) surfaces, comprising perfluorinated copper-phthalocyanines ($F_{16}$CuPc) and diindenoperylene (DIP). The electronic and crystalline properties have been addressed by means of scanning tunnelling microscopy (STM), synchrotron radiation spectroscopy measurements including valence-band (UPS), high resolution core-level photoelectron spectroscopy (XPS), as well as near edge X-ray absorption fine structure (NEXAFS), and state-of-the-art ab-initio calculations.


Figure 1. STM images depicting the crystalline structure of single component DIP, $F_{16}$CuPc as well as of binary layers. Superimposed on the images are the projected density of states on the respective occupied and unoccupied molecular orbitals closest to the Fermi edge. Their pronounced change of width gives evidence of the modified electronic coupling with the substrate in the mixed layer.

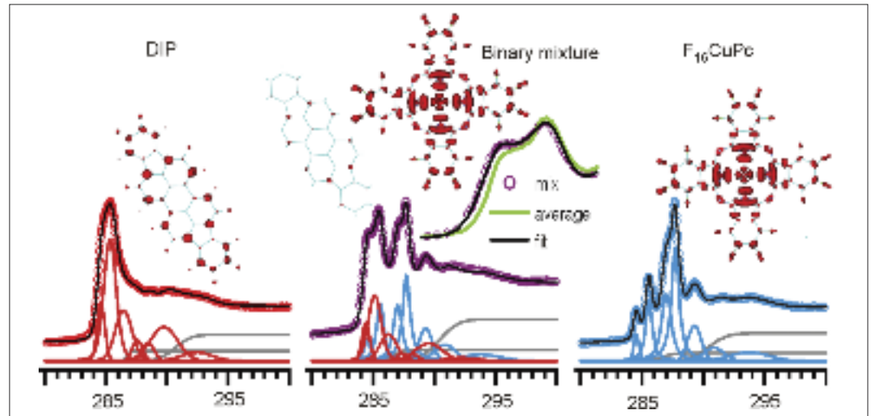


Figure 2. Experimental (symbols) and fitted (lines) C K-edge NEXAFS spectra of single component DIP, $F_{16}$CuPc and binary layers, together with the fit components. For the binary mixture, a zoom into the absorption edge region evidences the shift of the experimental spectra (in particular of the DIP components) with respect to the expected curve (average of $F_{16}$CuPc and DIP spectra) if no electronic changes took place in the mixture. Additionally shown are the calculated differences in electronic density with respect to the isolated molecules for $F_{16}$CuPc and DIP in the single-component and binary layers. The major changes upon molecular mixture take place for DIP, showing a reduced charge transfer.

Upon deposition of both molecules on the clean surface, these mix into a highly crystalline binary layer (Fig. 1), independently of whether the molecules are co-deposited or evaporated sequentially. The driving force behind this pronounced tendency to mix can be found in the greatly enhanced intermolecular interactions arising from the formation of multiple C-H···F-C hydrogen bonds in the binary layers. Most interestingly, the modified intermolecular interactions are accompanied by changes in the electronic coupling between molecules and substrate. In reference to the associated single component layers, the new supramolecular environment of the binary mixture causes the donor molecule (DIP) to decouple electronically from the metal surface, while the acceptor ($F_{16}$CuPc) suffers strong hybridization with the substrate (Fig. 1). The former causes the DIP-Cu(111) charge transfer to decrease, as evidenced by XPS and NEXAFS, and further supported by theoretical calculations (Fig. 2). UPS measurements and calculations also show how the $d_{3z^2-r^2}$ –like wave-functions of the Cu atoms in close contact with the organic overlayer hybridize with the $F_{16}$CuPc in the binary layer.

With this work we shed new light on the complex correlations between intermolecular and molecule–substrate interactions, and thereby take a step forward towards a better understanding of the self-assembly processes on surfaces.